

Resolving the decades-long transient FIRST J141918.9+394036: an orphan long gamma-ray burst or a young magnetar nebula?

B. MARCOTE,¹ K. NIMMO,^{2,3} O. S. SALAFIA,^{4,5,6} Z. PARAGI,¹ J. W. T. HESSELS,^{2,3} E. PETROFF,³ AND R. KARUPPUSAMY⁷

¹*Joint Institute for VLBI ERIC, Oude Hoogeveensedijk 4, 7991 PD Dwingeloo, The Netherlands*

²*ASTRON, Netherlands Institute for Radio Astronomy, Oude Hoogeveensedijk 4, 7991 PD Dwingeloo, The Netherlands*

³*Anton Pannekoek Institute for Astronomy, University of Amsterdam, Science Park 904, 1098 XH Amsterdam, The Netherlands*

⁴*Università degli Studi di Milano-Bicocca, Dip. di Fisica “G. Occhialini”, Piazza della Scienza 3, 20126 Milano, Italy*

⁵*INAF - Osservatorio Astronomico di Brera, via E. Bianchi 46, 23807 Merate, Italy*

⁶*INFN - Sezione di Milano-Bicocca, Piazza della Scienza 3, 20126 Milano, Italy*

⁷*Max-Planck-Institut für Radioastronomie, Auf dem Hügel 69, D-53121 Bonn, Germany*

(Received XXX; Revised XXX; Accepted XXX)

Submitted to ApJL

ABSTRACT

Ofek (2017) identified FIRST J141918.9+394036 (hereafter FIRST J1419+3940) as a radio source sharing similar properties and host galaxy type to the compact, persistent radio source associated with the first known repeating fast radio burst, FRB 121102. These bursts are thought to be produced by a young, rapidly spinning magnetar embedded in an environment which is remarkably similar to the ones where long gamma-ray bursts (GRBs) are produced. Law et al. (2018) showed that FIRST J1419+3940 is a transient source decaying in brightness over the last few decades. One possible interpretation is that FIRST J1419+3940 is a nearby analogue to FRB 121102 and that the radio emission represents a young magnetar nebula. Another interpretation is that FIRST J1419+3940 is an ‘orphan’ long GRB, seen off-axis. To distinguish between these hypotheses, we conducted radio observations using the European VLBI Network at 1.6 GHz to resolve the emission spatially and to search for millisecond-duration radio bursts. We detect FIRST J1419+3940 as a compact radio source with flux density $620 \pm 20 \mu\text{Jy}$ (on 2018 September 18) and a source size of 3.9 ± 0.7 mas (i.e. 1.6 ± 0.3 pc given the luminosity distance of 87 Mpc). These results confirm that the radio emission is non-thermal and imply an average expansion velocity of $(0.11 \pm 0.02)c$. Contemporaneous high-time-resolution observations using the 100-m Effelsberg telescope detected no millisecond-duration bursts of astrophysical origin. The source properties and lack of short-duration bursts are consistent with a GRB jet expansion, whereas they disfavor a magnetar birth nebula. We also confirm a steeper decline in the flux density emission during the last years, and provide possible explanations.

Keywords: radio continuum: transients – gamma-ray burst: individual: FIRST J1419+3940 – fast radio bursts – galaxies: dwarf – radiation mechanisms: non-thermal – techniques: high angular resolution

1. INTRODUCTION

Very-long-baseline radio interferometric (VLBI) observations are a powerful way to study astrophysical transients because they provide milliarcsecond angular resolution imaging and astrometry. Such transient

events can produce blast waves and slowly-evolving synchrotron afterglows, whose temporal evolution and interaction with the surrounding medium are well characterized by VLBI observations that can measure the projected size and proper motion of such emission.

This technique was successfully used to spatially resolve the emission and measure the expansion speed of the afterglow associated with the long gamma-ray burst (GRB) 030329 (Pihlström et al. 2007). VLBI

observations have also been used to study the first detected binary neutron star merger, GRB 170817A (Abbott et al. 2017). The obtained measurement of the proper motion and physical size constrained the nature of the source to be a relativistic jet (Mooley et al. 2018; Ghirlanda et al. 2018). Furthermore, VLBI observations contributed to the first precise localization of a fast radio burst (FRB), the repeating source FRB 121102 (Spitler et al. 2014, 2016; Scholz et al. 2016). The burst source was associated with a compact (< 0.7 pc; Marcote et al. 2017), persistent radio source with a luminosity of $\nu L_\nu \approx 3 \times 10^{38}$ erg s $^{-1}$ at 1.7 GHz (Chatterjee et al. 2017), located inside a low-metallicity star-forming region in a dwarf galaxy at a luminosity distance of 972 Mpc (Tendulkar et al. 2017; Bassa et al. 2017). The environment of FRB 121102 is remarkably similar to the ones where long GRBs are typically produced, favoring several scenarios that consider repeating FRBs to be produced by newly-born magnetars created during superluminous supernovae (see e.g. Margalit & Metzger 2018; Piro & Gaensler 2018). FRBs could thus be detectable at the sites of long GRBs, and the persistent source associated with FRB 121102 could be the longer-lived nebula following the afterglow of one of these events.

Based on the properties of FRB 121102’s persistent radio source and host galaxy, Ofek (2017) identified a number of similar sources in the Very Large Array (VLA) FIRST catalogue. Law et al. (2018) showed that one of these sources, FIRST J141918.9+394036 (hereafter FIRST J1419+3940) is a slowly declining transient. Using archival observations, they showed that the source declined from ~ 26 mJy (at 1.4 GHz) in 1993 to ≤ 0.4 mJy (at 3 GHz) in 2017. FIRST J1419+3940 is associated with a small star-forming galaxy at a luminosity distance of ~ 87 Mpc. Both the light-curve over the last ~ 25 yr and the inferred luminosities of $\nu L_\nu \gtrsim 3 \times 10^{38}$ erg s $^{-1}$ are consistent with the afterglow of a long GRB, requiring a released kinetic energy of $\sim 10^{51}$ erg at the time of the explosion. No convincing association with a previously detected GRB could be made, however (Law et al. 2018).

Alternatively, the fading radio emission could also be interpreted as coming from a new-born nebula powered by a young magnetar (Law et al. 2018). Indeed, FIRST J1419+3940’s properties and host galaxy are remarkably similar to the persistent radio counterpart and host galaxy of FRB 121102 (Ofek 2017). Both sources show similar environments and luminosities. Their physical nature could thus also be similar and FIRST J1419+3940 might be associated with a source capable of producing FRBs.

Here we present European VLBI Network (EVN) radio observations of FIRST J1419+3940 that provide the first constraints on the source compactness, coupled with simultaneous searches for millisecond-duration bursts. We present the observations and data reduction in Section 2. We describe the results in Section 3, and their implications for the nature of FIRST J1419+3940 in Section 4. Finally, we present our conclusions in Section 5.

2. OBSERVATIONS AND DATA REDUCTION

We observed FIRST J1419+3940 on 2018 September 18 between 12:00 and 19:00 UTC at 18 cm (1.6 GHz) with the EVN, involving a total of 12 stations: Jodrell Bank Mark2, Westerbork single-dish, Effelsberg, Medicina, Onsala 25-m, Tianma, Toruń, Hartebeesthoek, Sardinia, and three stations from e-MERLIN (Cambridge, Defford, and Knockin). The data were recorded with a total bandwidth of 128 MHz, and correlated in real time (e-EVN operational mode) at JIVE (The Netherlands) using the SFXC software correlator (Keimpema et al. 2015). The data were divided into eight subbands of 64 channels each, with full circular polarization, and 1-s time averaging. We also buffered the baseband EVN data in parallel to produce high-time-resolution correlations afterwards, if required.

Furthermore, we simultaneously observed FIRST J1419+3940 in the frequency range 1580–1736 MHz using the 100-m Effelsberg telescope and the PSRIX backend recorder (Lazarus et al. 2016). We recorded with two linear polarizations, achieving a gain of 1.5 K Jy $^{-1}$ and a receiver temperature of 25 K. The total bandwidth of 156 MHz was divided into 10 subbands — each one further divided into 64 channels and recorded with 32-bit time samples. The ultimate time and frequency resolution of the data were 40.96 μ s and 0.2438 MHz, respectively. Before processing, the subbands were combined into a single band and the data were converted to 4-bit samples to ensure compatibility with the PRESTO pulsar analysis software suite (Ransom 2001).

2.1. Interferometric data

We observed J1642+3948 as fringe finder and J1419+3821 (located at only 1.3° from FIRST J1419+3940) as phase calibrator. We scheduled a phase-referencing cycle of 4.5 min on the target and 1.5 min on the phase calibrator, achieving a total time of ~ 4.5 h on FIRST J1419+3940.

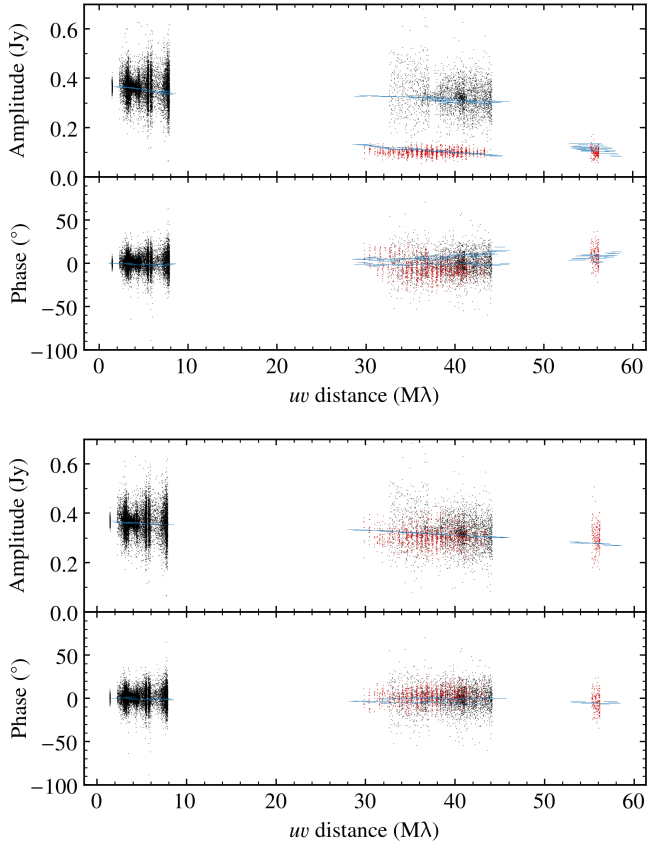


Figure 1. The obtained visibility data (amplitudes and phases) for the phase calibrator source, J1419+3821, after the original calibration (top) and in the alternate calibration where the gain calibration of the Tianma station was calibrated using a source model from only the stations with a robust amplitude calibration (bottom). See Sect. 2 for details. Red dots represent data from the baselines including the Tianma station. Blue lines represent the source model in each case.

The interferometric data were reduced using AIPS¹ (Greisen 2003) and Difmap (Shepherd et al. 1994) following standard procedures. A-priori amplitude calibration was performed using the known gain curves and system temperature measurements recorded individually on each station during the observation. We used nominal system equivalent flux density (SEFD) values for the following stations: Jodrell Bank Mark2, Tianma, and the e-MERLIN stations. We manually flagged data affected by radio frequency interference (RFI) and then we fringe-fitted and bandpass-calibrated the data using the fringe finder and the phase calibrator. We imaged and

self-calibrated the phase calibrator in Difmap to improve the final calibration of the data. The obtained solutions were then transferred to the target, which was finally imaged.

We note that Tianma did not produce reliable system temperature values during the experiment, therefore we used the nominal SEFD for amplitude calibration. This typically produces a satisfactory a-priori calibration that can be further improved during imaging and self-calibration. Tianma, however, provides the longest East-West baselines in our array with no equivalent baselines to compare with, and it also does not have short spacings to establish a reliable station calibration. In this case imaging and parametrization of source properties by model-fitting is complicated due to the fact that some source parameters may correlate with the Tianma station gain (Natarajan et al. 2017).

Figure 1 displays the visibility amplitudes and phases as a function of projected baseline length in units of observing wavelength. The top panel shows the initial calibration, with the Tianma data highlighted in red. The low amplitudes may be consistent with a source that is very compact in general, but well resolved in the East-West direction. The bottom panel shows the data after we apply an amplitude correction factor for Tianma, based on a source model obtained by only using the stations with robust calibration. The required scaling factor was about three, implying that the station could have been much less sensitive than expected.

Due to the uncertainty with the Tianma calibration, we decided to take the following procedure to analyze the data. Instead of fitting an elliptical-Gaussian model brightness distribution to the uv -data in model fitting, we assumed a circular-Gaussian brightness distribution. This is expected to be less sensitive to uncertainties of station gain calibration (Natarajan et al. 2017). In addition, we looked at the results derived from the following cases: Tianma removed from the data set, Tianma present with nominal gain calibration, and Tianma present but with its gain scaled to be in agreement with the most compact possible solution (as explained above). As we will see in Sect. 3, the fitted source sizes differ somewhat, but in all cases they support the same main conclusion: that our target is resolved on milliarcsecond scales.

2.2. High-time resolution data

The high-time-resolution Effelsberg data were analyzed to search for millisecond bursts or periodic signals. First, using PRESTO’s `rfifind`, we identified specific time and frequency channels contaminated by RFI. The regions highlighted by `rfifind` and the frequency

¹ The Astronomical Image Processing System (AIPS) is a software package produced and maintained by the National Radio Astronomy Observatory (NRAO).

range 1610–1631 MHz, associated with RFI from the Iridium satellites, were masked prior to conducting the analysis. We then dedispersed the 4-bit data using the PRESTO tool `prepsubband` for 2500 trial dispersion measures (DMs) in the range 0–1210.8 pc cm⁻³. The resulting dedispersed time series were then searched for single pulses above a 6- σ threshold using PRESTO’s `single_pulse_search.py`, which applies a matched-filter technique using boxcar functions and in our search was sensitive to burst durations in the range 40.96 and 1228.8 μ s. Dynamic spectra of the identified single-pulse candidates were generated and inspected by eye to distinguish between astrophysical signals and RFI.

In addition, a Fourier-domain search was performed on each individual dedispersed time series using PRESTO’s `accelsearch`, in order to search for periodic signals. Potential periodic signals were sifted using `ACCEL_sift.py`, and the remaining candidates were inspected by eye after folding using `prepfold`.

The RFI mitigation process was unable to remove all instances of RFI in the data. We calculate that of the ~ 4.3 -h Effelsberg on-source time, approximately 92.4% was examined for bursts and periodic signals. Note the discrepancy between the Effelsberg on-source time (~ 4.3 h) and the EVN on-source time (~ 4.5 h) which can be understood as Effelsberg slewing is slower than the average station.

The aforementioned analysis strategy was verified using similar data targeting pulsar PSR B2020+28.

3. RESULTS AND DISCUSSION

3.1. On the persistent emission

FIRST J1419+3940 is detected on 2018 September 18 as a radio source that is compact on milliarcsecond scales (see Fig. 2), with a flux density of 620 ± 20 μ Jy at a position of:

$$\begin{aligned}\alpha(\text{J2000}) &= 14^{\text{h}}19^{\text{m}}18.850722^{\text{s}} \pm 0.23 \text{ mas} \\ \delta(\text{J2000}) &= 39^{\circ}40'36.04520'' \pm 0.23 \text{ mas},\end{aligned}$$

where the quoted uncertainties take into account the statistical uncertainties in the image (0.2 mas in both α and δ), the uncertainty in the phase calibrator position (0.1 mas; Beasley et al. 2002; Gordon et al. 2016), and the estimated uncertainties associated with the phase referencing technique (0.06 and 0.04 mas for α and δ , respectively; Pradel et al. 2006). The obtained position is consistent with the one reported from the FIRST survey (Law et al. 2018), as well as the preliminary results published in Marcote et al. (2018). The measured flux density on 2018 September 18 is consistent with the declining trend of the light-curve reported from

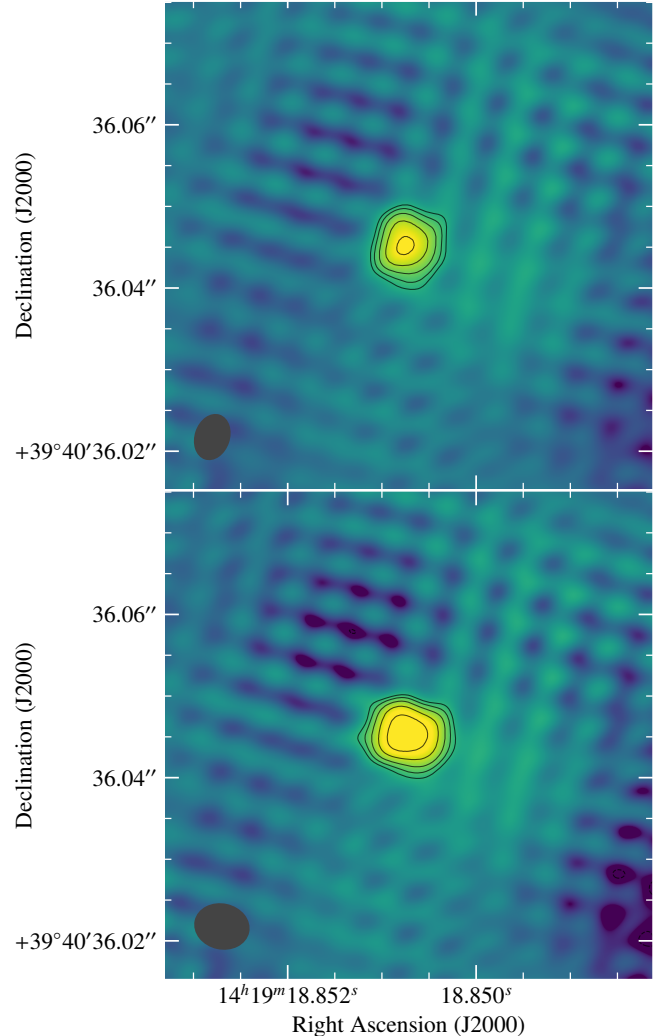


Figure 2. Images of FIRST J1419+3940 at 1.6 GHz with the EVN on 2018 September 18 derived from the two gain calibrations performed in Tianma (original, top, and scaled, bottom). Contours start at a 3- σ rms noise level of 25 and 29 μ Jy beam⁻¹, respectively, and increase by factors of $\sqrt{2}$. The synthesized beams are represented by the dark gray ellipses at the bottom left corner of each image.

observations with the Karl G. Jansky Very Large Array, VLA (see Fig. 3). In this sense, no significant emission seems to be resolved out between arcsecond scales (VLA data) and milliarcsecond scales (our EVN data). Given the luminosity distance of 87 Mpc, the obtained flux density corresponds to an isotropic luminosity $\nu L_\nu = (9.4 \pm 0.3) \times 10^{36}$ erg s⁻¹. Considering the last published VLA observation at 3.0 GHz, we can put an upper limit on the spectral index between 1.6 and 3.0 GHz of $\alpha \lesssim -0.62$ (where $S_\nu \propto \nu^\alpha$).

FIRST J1419+3940 is significantly resolved in the obtained images given the size of the synthesized beam

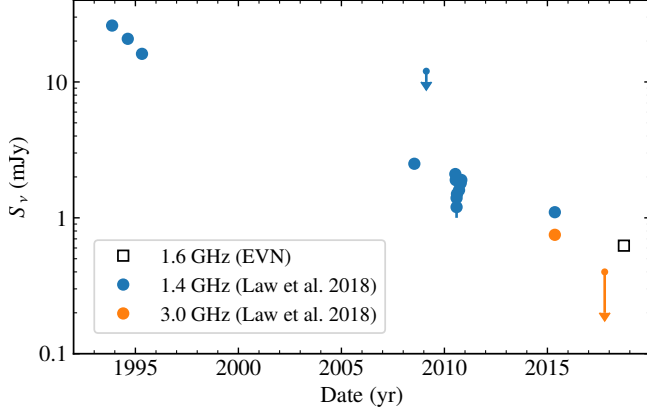


Figure 3. Light-curve of FIRST J1419+3940 during the last 25 yr at 1.4–1.6 GHz (blue circles and open square) and 3.0 GHz (orange circles). Errors bars represent $1\text{-}\sigma$ uncertainties (hidden by the size of the markers in most cases). Arrows represent $3\text{-}\sigma$ upper-limits.

($5.5 \times 4.1 \text{ mas}^2$), as the measured size is larger than the minimum resolvable size by the array (see Martí-Vidal et al. 2012; Natarajan et al. 2017, for a detailed explanation). By fitting a circular Gaussian to the uv data we measure a source size of $\approx 4.3 \text{ mas}$, with an estimated uncertainty of $\approx 20\%$. However, we note that the gain calibration of Tianma constitutes a potential source of systematic errors in the size measurement. To provide a more reliable measurement, we produced images without this station. Despite having poorer resolution (synthesized beam of $24 \times 5.3 \text{ mas}^2$), we obtained a size that is significant and consistent with the value quoted above ($\approx 3.9 \text{ mas}$). Finally, we imaged the source with the gain correction applied to Tianma (as mentioned in the previous section), which provides the most stringent lower limit on the source size. In this case we measured a source size of $\approx 3.4 \text{ mas}$. The contribution of the longest baselines is therefore not critical as we obtain consistent results from all cases. We summarize the results of these different analyses in Table 1.

For comparison, the phase calibrator, J1419+3821, exhibits a main point-like component with a measured size of 1.1–2.9 mas in all cases. This argues against the possibility that the measured size of FIRST J1419+3940 is due to scatter broadening from our Galaxy, as the two sources, FIRST J1419+3940 and J1419+3821 should then exhibit similar sizes.

We thus conclude that FIRST J1419+3940 is significantly resolved, with an angular size of $3.9^{+0.4+0.3}_{-0.5-0.2} \text{ mas}$, where the first uncertainties take into account the dispersion of the values from the different analyses, and the second ones consider the estimated statistical uncertainties on the value. Given that the luminosity distance to

the source is 87 Mpc (Law et al. 2018), we derive a projected physical size of $1.6 \pm 0.3 \text{ pc}$. This size also implies a brightness temperature of $T_b \sim 1.1 \times 10^7 \text{ K}$, which clearly points to a non-thermal origin for the emission.

Law et al. (2018) estimated that the putative GRB producing the observed afterglow likely took place around $\sim 25\text{--}30 \text{ yr}$ ago. Assuming these dates, the afterglow must have a mean expansion velocity of $v = (3.2 \pm 0.6) \times 10^4 \text{ km s}^{-1}$, or $\sim (0.11 \pm 0.02)c$, consistent with a mildly relativistic expansion (we note that in these 30 yr a significant deceleration is expected).

3.2. On the single burst searches

We detected no astrophysical single pulses or periodic signals in the high-time-resolution Effelsberg data. We can estimate the expected dispersion measure (DM) towards FIRST J1419+3940 using Galactic electron density models (NE2001; Cordes & Lazio 2002, YMW16; Yao et al. 2017). For an extragalactic source, the observed DM can be divided into four components along the line of sight:

$$\text{DM}_{\text{obs}} = \text{DM}_{\text{MW}} + \text{DM}_{\text{MW}_{\text{halo}}} + \text{DM}_{\text{IGM}} + \text{DM}_{\text{host}}. \quad (1)$$

The Milky Way contribution to the DM along the line of sight is divided into the disk and spiral arm component, DM_{MW} , and the Galactic halo component $\text{DM}_{\text{MW}_{\text{halo}}}$. The former, DM_{MW} , is 44.22 and 38.51 pc cm^{-3} calculated using the NE2001 and YMW16 models, respectively. The uncertainties in these contributions are not well quantified, but are likely on the order of 20%. Using this, we can derive an approximate range of: $30.81 \lesssim \text{DM}_{\text{MW}} \lesssim 53.06 \text{ pc cm}^{-3}$. The Galactic halo contributes $\sim 30 \text{ pc cm}^{-3}$ to the DM (Dolag et al. 2015). Given that the redshift of FIRST J1419+3940 is 0.01957 (Law et al. 2018), the mean intergalactic medium (IGM) contribution to the DM is $\text{DM}_{\text{IGM}} \approx 20 \text{ pc cm}^{-3}$ (Ioka 2003; Inoue 2004). We assume that the DM contribution of the host galaxy of FIRST J1419+3940, DM_{host} , is comparable to that of the host galaxy of FRB 121102: $55 \lesssim \text{DM}_{\text{host}} \lesssim 225 \text{ pc cm}^{-3}$ (Tendulkar et al. 2017). Combining all individual components using equation (1) results in $135.81 \lesssim \text{DM}_{\text{obs}} \lesssim 328.06 \text{ pc cm}^{-3}$.

From the single pulse candidates reported using `single_pulse_search.py`, an astrophysical burst would be identifiable provided the signal-to-noise ratio exceeds ~ 10 . We can estimate the fluence limit of our search using

$$F = (S/N)_{\text{min}} \frac{T_{\text{sys}}}{G} \sqrt{\frac{W_b}{n_{\text{pol}} \Delta \nu}} \quad (2)$$

(following Cordes & McLaughlin 2003), where $(S/N)_{\text{min}}$ is our detection threshold of 10, T_{sys} is the system temperature, G is the telescope gain, n_{pol} is the number of

Table 1. Properties of FIRST J1419+3940 measured following different imaging approaches.

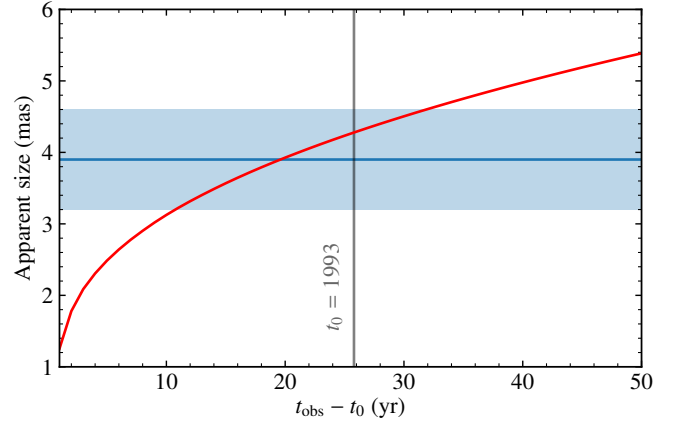
	rms	Peak	Flux	size	synthesized beam
	($\mu\text{Jy beam}^{-1}$)	($\mu\text{Jy beam}^{-1}$)	(μJy)	(mas)	(mas \times mas, $^\circ$)
Default calibration	19	300	620	4.3	5.5×4.1 , -18°
Without Tianma	30	510	630	3.9	24×5.3 , 75°
Corrected Tianma	25	459	624	3.4	6.6×5.4 , 78°

recorded polarizations, $\Delta\nu$ is the total bandwidth, and W_b is the observed width of the burst. The observed width, W_b , accounts for broadening of the intrinsic width due to the finite time sampling of the data, intra-channel smearing, smearing due to DM-trial spacing, and scatter broadening. FRB 121102 has been shown to exhibit individual bursts with widths $\lesssim 30 \mu\text{s}$ (Michilli et al. 2018) and there have been observations of FRBs with widths as large as $\sim 30 \text{ ms}$ (Petroff et al. 2016)². Taking a DM of 200 pc cm^{-3} and intrinsic widths $30 \mu\text{s}$ – 30 ms , we find our fluence limit ranges from 0.1 Jy ms to 8.1 Jy ms .

4. INTERPRETATION

4.1. Measured source size

In order to compare our measurements with the scenarios proposed by Law et al. (2018), we need to compute the expected apparent size of the source. At the time of our observation, $t_{\text{obs}} \sim 30 \text{ yr} \sim 10^4 \text{ d}$ after the initial explosion, the external shock produced by the GRB jet upon deceleration into the interstellar medium (ISM) is expected to be non-relativistic, and to have turned quasi-spherical (the transition to the Sedov-Taylor phase happens at $t_{\text{ST}} \sim 200 \text{ d}$, e.g. Sironi & Giannios 2013). The initial relativistic expansion phase, however, can still have effects on the relation between observed time and projected size. For that reason, we compute the jet deceleration dynamics and spreading employing the “trumpet” model from Granot & Piran (2012), which has been shown to be in good quantitative agreement with results from numerical relativistic hydrodynamics simulations. The observed size is estimated as the maximum projected size of the equal-arrival-time surface, relativistic beaming of radiation being negligible in our late-time observations. Using the same jet parameters as Law et al. (2018), namely an isotropic equivalent energy $E_{\text{iso}} = 2 \times 10^{53} \text{ erg}$, an ISM number density $n = 10 \text{ cm}^{-3}$ and a viewing angle $\theta_v = 0.6 \text{ rad}$, and further assuming a

**Figure 4.** Source apparent size evolution. The red line shows the predicted apparent size evolution for a jet with parameters as those proposed by Law et al. (2018). The blue line and the lighter blue band show our measured apparent size and its $1\text{-}\sigma$ uncertainty of $\theta_s = 3.9 \pm 0.7 \text{ mas}$. The grey vertical line marks the source age at the time of our observation, assuming that it originally exploded in 1993.

jet half-opening angle $\theta_j = 0.1 \text{ rad}$ (which implies a total jet energy $E_{\text{jet}} \sim 10^{51} \text{ erg}$), we obtain the size evolution shown by the red solid line in Fig. 4, which is fully compatible with the measured one, assuming that the GRB took place in 1993. This disfavors the alternative scenario of a magnetar birth nebula, which would have not reached such a large size, due to the much lower expansion velocity.

4.2. Flux density

While the measured size agrees well with the GRB scenario proposed by Law et al. (2018), our measured flux density $S_{1.6 \text{ GHz}} = 620 \pm 20 \mu\text{Jy}$ is low when compared to the extrapolation of their model. More precisely, adopting the same assumptions as Law et al. (2018), namely quasi-isotropic, adiabatic expansion, Deep Newtonian regime and an electron power law index $p = 2.2$, the flux density should follow $S_\nu \propto \nu^{-0.6} t^{-0.96}$. Using the latest VLA detection as reference, which yielded a flux density of $1.1 \pm 0.1 \text{ mJy}$ at 1.52 GHz on 2015 May 11, and assuming the GRB to have happened in 1993, we

² All published FRBs and their properties can be found in the FRB Catalogue: <http://www.frbcat.org>

should have measured $S_{1.6\text{GHz}} \approx 930 \pm 85 \mu\text{Jy}$ at the time of our observation, which is $\sim 3.5\sigma$ (summing the uncertainties in quadrature) above our measured flux density. As noted by Law et al. (2018), the latest VLASS non-detection $S_\nu < 400 \mu\text{Jy}$ at 3 GHz on 2017.78 already pointed to a faster decline after 2015. Several physical processes could lead to a steepening in the decay of the lightcurve, e.g.:

- The conditions in the shocked fluid could be changing as a consequence of the transition to the non-relativistic, Deep Newtonian phase, e.g. the fraction ϵ_e of shock energy given to electrons could decrease, or the electron momentum distribution power law index p could decrease from $p = 2.2$ towards ~ 2 (Sironi & Giannios 2013). Both these effects would result in a steepening of the flux decay;
- Contrary to what stated by Law et al. (2018), the steepening could also be due to the shock crossing a dip in the ISM density. According to the argument by Law et al. (2018), based on Nakar & Granot (2007) and Mimica & Giannios (2011), an ISM density drop would result only in a smooth, slow change in the lightcurve. This is essentially a consequence of the assumption that the shock is relativistic ($\Gamma \gg 1$), in which case the angular time scale $R/2\Gamma^2 c$ would be of the same order as the observer time t_{obs} , and therefore any change in the shock conditions would be smeared out over that time scale. In our case, conversely, the shock expansion speed is non-relativistic, and the angular time scale is $\sim R/2c \ll t_{\text{obs}}$ (using our size measurement, we have $R/c \sim 2.5 \text{ yr}$, which is significantly smaller than the explosion age $t_{\text{obs}} \gtrsim 25 \text{ yr}$), so that a drop in the ISM density at a radius slightly smaller than the observed size $\sim 1.6 \text{ pc}$ would justify the flux deficit. Such a drop could mark the outer radius of the star-forming region where the GRB exploded.

The flux deficit cannot be understood as due to scintillation-induced fluctuations, as the apparent size of the source is too large (Goodman 1997).

4.3. Comparison with PTF10hgi

Recently, a radio source was discovered coincident with the superluminous supernova PTF10hgi (Eftekhari et al. 2019). An off-axis jet is explored as the potential origin of the emission, but is considered unlikely due to the high inferred isotropic jet energy, exceeding that of most observed long GRBs. However, the

inferred properties of the radio source associated with PTF10hgi ($E_{\text{iso}} \sim (3-5) \times 10^{53} \text{ erg}$, $n = 10^{-3}-10^2 \text{ cm}^{-3}$; Eftekhari et al. 2019) are comparable to the estimates for FIRST J1419+3940 ($E_{\text{iso}} = 2 \times 10^{53} \text{ erg}$, $n = 10 \text{ cm}^{-3}$; Law et al. 2018). The results shown in this work support the scenario in which FIRST J1419+3940 is an orphan GRB afterglow, thus favoring the hypothesis that the radio source associated with PTF10hgi has a similar origin. This, further, supports the idea that FIRST J1419+3940 was created as the result of a superluminous supernova. Conducting VLBI radio observations to resolve the radio emission associated with PTF10hgi will aid in testing the parallels between this source and FIRST J1419+3940.

4.4. Comparison with FRB 121102

The characteristics of FIRST J1419+3940 reported by Law et al. (2018) match those of the persistent source associated with FRB 121102: i.e., a compact radio source with a similar luminosity and co-located with a star-forming region of a dwarf galaxy. Whereas the lightcurve of FIRST J1419+3940 is declining, as opposed to the persistent emission from FRB 121102 (Chatterjee et al. 2017, Plavin et al. in prep), this could naturally be explained by a younger age (~ 30 instead of $\sim 50-100 \text{ yr}$, e.g. Piro & Gaensler 2018).

The obtained source size is significantly larger than the one associated to FRB 121102 ($< 0.7 \text{ pc}$; Marcote et al. 2017), implying a much higher expansion velocity. However, we note that proposed FRB scenarios (see e.g. Margalit & Metzger 2018; Piro & Gaensler 2018) consider typical mean ejecta speeds of $\sim 10^{3-4} \text{ km s}^{-1}$. The value derived for FIRST J1419+3940 is thus close to, but above, the highest end of this range.

Metzger et al. (2017) argue that the age of FRB 121102 is at most 100 yr if the progenitor of the bursts is a millisecond magnetar. This is comparable to the estimated age ($\sim 30 \text{ yr}$) of FIRST J1419+3940 (Law et al. 2018). In this scenario one would expect that bursts from FIRST J1419+3940 are similar to FRB 121102. Bursts from the repeating FRB 121102 have been observed with fluences of $\sim 0.02 \text{ Jy ms}$ (Gajjar et al. 2018) to $\sim 1.2 \text{ Jy ms}$ (Spitler et al. 2014) and widths ranging from $\lesssim 30 \mu\text{s}$ (Michilli et al. 2018) to $\sim 8.7 \text{ ms}$ (Spitler et al. 2016). Taking this range of fluence values at the luminosity distance of FRB 121102 (972 Mpc) and scaling to the luminosity distance of FIRST J1419+3940 (87 Mpc), gives an estimated fluence range of 2.5–150 Jy ms. For bursts with widths exceeding $\sim 9 \text{ ms}$, the fluence limit of our search increases beyond 2.5 Jy ms (see Section 3.2). Under the assumption that FIRST J1419+3940 is producing bursts with widths comparable to that of

FRB 121102 and with an alignment (with respect to the observer) consistent with FRB 121102, single bursts from this source would be identifiable in the data.

Recently, a second repeating FRB was discovered, FRB 180814.J0422+73 (Amiri et al. 2019). An upper limit of ~ 500 Mpc has been placed on the distance to the source. If FIRST J1419+3940 produces bursts similar to FRB 180814.J0422+73 ($\sim 3\text{--}100$ Jy ms at ~ 500 Mpc), the bursts would have fluences of $\sim 100\text{--}3300$ Jy ms, which well exceeds the fluence limit of our search.

The result that we found no single bursts can be understood in a number of scenarios: (a) FIRST J1419+3940 does not produce bursts; (b) FIRST J1419+3940 produces beamed single bursts that are off-axis, and therefore do not cross our line-of-sight; (c) like FRB 121102 (Gajjar et al. 2018), FIRST J1419+3940 could experience periods where no bursts are observed, either due to the source “switching off”, or only producing weak bursts with fluences below our detection threshold. To ensure our search was not affected by self-absorption, future observations of FIRST J1419+3940 at higher radio frequencies are required.

5. CONCLUSIONS

FIRST J1419+3940 was reported as a slowly fading radio transient source. We provide the first constraints on the source size, using EVN data. These measurements confirm the non-thermal emission of the source and are consistent with jet expansion from a putative orphan long GRB. A flux density lower than expected is reported, suggesting a faster decline after 2015. This decay could be explained by a change in the post-shock microphysical parameters following the transition to the non-relativistic phase, or by a drop in the ISM density (e.g. due to the shock reaching the outer edge of the star-forming region where the GRB exploded). We exclude scintillation-induced fluctuations as the origin of the reported variability.

Finally, although FIRST J1419+3940 exhibited similar properties as the persistent source associated with FRB 121102, we note significant differences (e.g. FIRST J1419+3940 shows a much faster expansion, and stronger luminosity decay). Still, FIRST J1419+3940 could be a site of potential FRB production, although the burst searches conducted during the EVN observation reported null results.

ACKNOWLEDGEMENTS

We thank H. J. van Langevelde for an internal review of the manuscript. The European VLBI Network is a joint facility of independent European, African, Asian, and North American radio astronomy institutes. Scientific results from data presented in this publication are derived from the following EVN project code: RM015. e-MERLIN is a National Facility operated by the University of Manchester at Jodrell Bank Observatory on behalf of STFC. We thank the directors and staff of all the EVN telescopes for making this target of opportunity observation possible. We thank the staff of the Effelsberg Radio Telescope, and in particular U. Bach, for his support with simultaneous pulsar recording. O.S. wishes to thank G. Ghirlanda for valuable discussions and insights. B.M. acknowledges support from the Spanish Ministerio de Economía y Competitividad (MINECO) under grants AYA2016-76012-C3-1-P and MDM-2014-0369 of ICCUB (Unidad de Excelencia “María de Maeztu”). J.W.T.H. acknowledges funding from an NWO Vidi fellowship and from the European Research Council under the European Union’s Seventh Framework Programme (FP/2007-2013) / ERC Starting Grant agreement nr. 337062 (“DRAGNET”). R.K. is supported by the ERC synergy grant “BlackHoleCam: Imaging the Event Horizon of Black Holes” (Grant No. 610058). This research made use of APLpy, an open-source plotting package for Python hosted at <http://aplpy.github.com>, Astropy, a community-developed core Python package for Astronomy (Astropy Collaboration et al. 2013), and Matplotlib (Hunter 2007).

REFERENCES

- Abbott B. P., et al., 2017, *ApJ*, **848**, L12
 Amiri M., et al., 2019, *Nature*
 Astropy Collaboration et al., 2013, *A&A*, **558**, A33
 Bassa C. G., et al., 2017, *ApJL*, **843**, L8
 Beasley A. J., Gordon D., Peck A. B., Petrov L., MacMillan D. S., Fomalont E. B., Ma C., 2002, *ApJS*, **141**, 13
 Chatterjee S., et al., 2017, *Nature*, **541**, 58
 Cordes J. M., Lazio T. J. W., 2002, arXiv Astrophysics e-prints,
 Cordes J. M., McLaughlin M. A., 2003, *ApJ*, **596**, 1142
 Dolag K., Gaensler B. M., Beck A. M., Beck M. C., 2015, *MNRAS*, **451**, 4277
 Eftekhari T., et al., 2019, arXiv e-prints,
 Gajjar V., et al., 2018, *ApJ*, **863**, 2
 Ghirlanda G., et al., 2018, preprint, p. arXiv:1808.00469 (arXiv:1808.00469)
 Goodman J., 1997, *NewA*, **2**, 449
 Gordon D., et al., 2016, *AJ*, **151**, 154

- Granot J., Piran T., 2012, *MNRAS*, **421**, 570
- Greisen E. W., 2003, in Heck A., ed., *Astrophysics and Space Science Library* Vol. 285, Information Handling in Astronomy - Historical Vistas. p. 109, doi:10.1007/0-306-48080-8_7
- Hunter J. D., 2007, *Computing In Science & Engineering*, **9**, 90
- Inoue S., 2004, *MNRAS*, **348**, 999
- Ioka K., 2003, *ApJL*, **598**, L79
- Keimpema A., et al., 2015, *Experimental Astronomy*, **39**, 259
- Law C. J., Gaensler B. M., Metzger B. D., Ofek E. O., Sironi L., 2018, *ApJ*, **866**, L22
- Lazarus P., Karuppusamy R., Graikou E., Caballero R. N., Champion D. J., Lee K. J., Verbiest J. P. W., Kramer M., 2016, *MNRAS*, **458**, 868
- Marcote B., et al., 2017, *ApJL*, **834**, L8
- Marcote B., Paragi Z., Hessels J. W. T., 2018, *The Astronomer's Telegram*, **12126**, 1
- Margalit B., Metzger B. D., 2018, *ApJ*, **868**, L4
- Martí-Vidal I., Pérez-Torres M. A., Lobanov A. P., 2012, *A&A*, **541**, A135
- Metzger B. D., Berger E., Margalit B., 2017, [arXiv170102370M],
- Michilli D., et al., 2018, *Nature*, **553**, 182
- Mimica P., Giannios D., 2011, *MNRAS*, **418**, 583
- Mooley K. P., et al., 2018, *Nature*, **561**, 355
- Nakar E., Granot J., 2007, *MNRAS*, **380**, 1744
- Natarajan I., Paragi Z., Zwart J., Perkins S., Smirnov O., van der Heyden K., 2017, *MNRAS*, **464**, 4306
- Ofek E. O., 2017, *ApJ*, **846**, 44
- Petroff E., et al., 2016, *PASA*, **33**, e045
- Pihlström Y. M., Taylor G. B., Granot J., Doeleman S., 2007, *ApJ*, **664**, 411
- Piro A. L., Gaensler B. M., 2018, *ApJ*, **861**, 150
- Pradel N., Charlot P., Lestrade J.-F., 2006, *A&A*, **452**, 1099
- Ransom S. M., 2001, PhD thesis, Harvard University
- Scholz P., et al., 2016, *ApJ*, **833**, 177
- Shepherd M. C., Pearson T. J., Taylor G. B., 1994, in *Bulletin of the American Astronomical Society*. p. 987
- Sironi L., Giannios D., 2013, *The Astrophysical Journal*, **778**, 107
- Spitler L. G., et al., 2014, *ApJ*, **790**, 101
- Spitler L. G., et al., 2016, *Nature*, **531**, 202
- Tendulkar S. P., et al., 2017, *ApJL*, **834**, L7
- Yao J. M., Manchester R. N., Wang N., 2017, *ApJ*, **835**, 29